TÜBİTAK

Turkish Journal of Physics

http://journals.tubitak.gov.tr/physics/

Research Article

Turk J Phys
(2015) 39: 60 – 68
© TÜBİTAK
doi:10.3906/fiz-1405-13

Analysis and simulation of semiconductor laser dynamics with optoelectronic delay feedback

Varghese BEJOY[1,*], **Sivasankaran RAJESH**[2], **Vadakkedath Madhom NANDAKUMARAN**[1,3]
[1]International School of Photonics, Cochin University of Science and Technology, Kochi, India
[2]Department of Physics, N.S.S. College, Pandalam, Pathanamthitta, India
[3]Department of Physics, Amrita School of Arts and Sciences, Amrita Viswavidyapeetham, Kollam, India

Received: 23.05.2014 • **Accepted:** 25.08.2014 • **Published Online:** 23.02.2015 • **Printed:** 20.03.2015

Abstract: In this work we investigate semiconductor laser dynamics with optoelectronic delay feedback, both analytically and numerically. Stability criteria are derived from the delay differential equations of the system. Stability curves are obtained in the feedback strength–delay parameter space. We show that delay has a role in determining the stability only for a range of feedback strength and this range can vary depending on other parameters. Effects of bias current and nonlinear gain reduction on the stability curves are shown in the analysis and numerically verified.

Key words: Semiconductor laser, delay feedback, stability, Hopf bifurcation

1. Introduction

Semiconductor lasers (SLs) with delayed feedback have been investigated extensively in recent years, due to the rich variety of nonlinear phenomena they exhibit and also because of their potential applications [1]. They are excellent dynamical models that show many exciting phenomena such as low and high dimensional chaos [2], local and global bifurcations [3], control [4] and synchronization of chaos [5,6], intensity instabilities [7], multistability and hysteresis [8], and stochastic resonance effects [9,10]. Incorporating time delay into the system makes it infinite dimensional and consequently the system can exhibit very complex dynamics. Many aspects of delay dynamics have been observed and studied first in laser systems [1,11]. These nonlinear effects in semiconductor lasers have novel technological applications like secure information encryption [9,12] and chaotic lidar [13]. Modification of laser dynamics with feedback depends on many factors such as type and strength of feedback, delay time involved in the feedback mechanism, bias current, and other parameters like gain nonlinearities. Feedback mechanism can be either optical [14,15] or optoelectronic [16,17]. In optical feedback, a part of the output laser field is injected back into the laser cavity. The other technique involves a high bandwidth photodetector for optoelectronic conversion of the laser output and the injection of a suitably amplified detector signal into the pumping current of the SL. Even when the nonlinear gain reduction is strong enough to inhibit period doubling and chaos in current modulated semiconductor lasers [18], delay feedback has been proved to induce bifurcations and chaos [19]. Destabilization of the fixed point by Hopf bifurcation in SLs with optoelectronic feedback has been reported in many works [15,17]. Given such considerations, it is of utmost importance for the system designer to know how the SL stability varies with feedback and changes with different parameters. In this work, we analyze the delay differential equations of the SL with optoelectronic

*Correspondence: bejoyrosily@gmail.com

delay feedback to study the dependence of Hopf bifurcation phenomena on the nonlinear gain reduction factor, for a range of values of feedback strength and bias current. In addition, the effect of initial condition on the dynamics is studied by switching on the delay mechanism at different stages in the operation of the laser.

2. Model and analysis

In optoelectronic delay feedback the phase of the output optical field is not involved in determining the system dynamics. Therefore, the dynamics can be studied using 2 rate equations, one for carrier density (N) and the other for photon density (P). Single mode rate equations of an SL are given by [18,20]

$$\frac{dN}{dt} = \frac{1}{\tau_e}\left(\frac{I}{I_{th}} - N - \frac{N-\delta}{1-\delta}P\right) \tag{1}$$

$$\frac{dP}{dt} = \frac{1}{\tau_p}\left(\frac{N-\delta}{1-\delta}(1-\varepsilon P)P - P + \beta N\right), \tag{2}$$

where I is the total pumping current, I_{th} is threshold laser current, and τ_e and τ_p are the electron and photon lifetimes, respectively. $\delta = \mathrm{n}_0/\mathrm{n}_{th}$, n_0 is the carrier density required for transparency and n_{th} is the threshold carrier density. ε is related to the nonlinear gain reduction factor ε_{NL} by the equation [18]

$$\varepsilon = \varepsilon_{NL}\Gamma\left(\frac{\tau_e}{\tau_p}\right)n_{th}. \tag{3}$$

is the confinement factor. β is the spontaneous emission factor. When optoelectronic feedback is introduced the total pumping current at any instant of time becomes

$$I(t) = I_b + FP(t-\tau). \tag{4}$$

Here I_b is the constant bias current, F is the feedback strength, and τ represents the delay in feedback. This delay can arise from time taken for external transit of the laser beam and finite response time of the detector as well as the intentional delays included in the feedback circuitry. The values of the parameters are chosen as $\tau_p = 6$ ps, $\tau_e = 3$ ns, $\delta = 0.692$, $\beta = 5.0 \times 10^{-5}$ [18].

To determine the stability of the fixed point of the system consisting of Eqs. (1) and (2), the nature of the roots of the characteristic equation has to be calculated. The characteristic equation of a delay differential system is a transcendental equation that admits several solutions, given by [11]

$$\left|J_0 + e^{-\lambda\tau}J_\tau - \lambda I\right| = 0, \tag{5}$$

where J_0 is the Jacobian with respect to the present variables, J_τ is the Jacobian with respect to the delayed variables evaluated at the equilibrium point, and λs are the eigen values with $\lambda = \alpha + \mathrm{i}\gamma$. If all of the eigenvalues of the characteristic equation have negative real parts, then the equilibrium point is said to be stable. On the other hand, if at least one of the eigenvalues has a positive real part, then the equilibrium point is unstable. The characteristic equation for our set of rate equation becomes

$$\lambda^2 + K_2\lambda + K_3 + K_4e^{-\lambda\tau} = 0, \tag{6}$$

where

$$K_2 = \left(\frac{1}{\tau_e}\right)\left[1 + \frac{P_0}{(1-\delta)}\right] - \frac{(N_0 - 1 - 2\varepsilon P_0(N_0-\delta))}{\tau_p(1-\delta)} \tag{7}$$

$$K_3 = \frac{-1}{\tau_e \tau_p (1-\delta)} \left[\left(1 + \frac{P_0}{(1-\delta)} \right) (N_0 - 1 - 2\varepsilon P_0 (N_0 - \delta)) + \left(\varepsilon P_0^2 - P_0 - \beta (1-\delta) \right) \left(\frac{N_0 - \delta}{1-\delta} \right) \right] \tag{8}$$

$$K_4 = \frac{-F}{\tau_e \tau_p I_{th} (1-\delta)} \left[-\varepsilon P_0^2 + P_0 + \beta (1-\delta) \right]. \tag{9}$$

A change in stability can occur only when a root of Eq. (5) crosses the imaginary axis, that is when the real part of the eigenvalue changes from negative to positive, where λ with $\alpha = 0$ is a solution of the equation. Substituting $\alpha = 0$ in Eq. (6) and equating the real and imaginary parts of the resulting equation we get

$$K_2 \gamma - K_4 sin(\gamma\tau) = 0 \tag{10}$$

and

$$-\gamma^2 + K_3 + K_4 cos(\gamma\tau) = 0, \tag{11}$$

which leads to

$$\tau_{\pm.} = \frac{\pm arccos\left(\left[\frac{\gamma^2 - K_3}{K_4} \right] \right) + 2n\pi}{\gamma}, \tag{12}$$

where n is an integer. Squaring and adding Eqs. (10) and (11) result in a fourth degree equation in γ

$$\gamma^4 + \gamma^2 \left(K_2^2 - 2K_3 \right) + \left(K_3^2 - K_4^2 \right) = 0. \tag{13}$$

This equation is solved to find the range of F, where γ^2 is real and positive. $\tau_{\pm}$ are calculated using Eq. (12) for these values of F. Both τ_- and τ_+ satisfy the characteristic equation for $\alpha = 0$. The results we present in this work are specific to 2 types of feedback schemes: when feedback starts after the SL has stabilized to steady state operation and when feedback is present from the beginning of SL operation. In the first scheme the bifurcations happen on τ_-, but feedback can be applied in many possible ways, of which one may lead to bifurcations on τ_+. As delay systems generally exhibit abundant multistability, to devise such a unique scheme can be difficult. Since the feedback schemes we use in this work do not give bifurcations on τ_+, in the following discussions we assume

$$\tau_i (n) = \frac{-arccos\left(\frac{\gamma_i^2 - K_3}{K_4} \right) + 2n\pi}{\gamma_i}, \tag{14}$$

i = 1,2 corresponding to 2 real and positive solutions of Eq. (13). Negative or imaginary values of γ will yield τ_i(n)'s that are unphysical. These are the critical values of delay (τ_c) where the stability changes. To find the direction in which the eigen value crosses the imaginary axis, $d\alpha/d\tau$ is calculated on each τ(n). If $d\alpha/d\tau$ is positive, at delay equal to τ_i(n), the eigenvalue crosses the imaginary axis to the positive side as the delay is increased and the fixed point becomes unstable. If $d\alpha/d\tau$ is negative at τ_i(n), the eigen value crosses the imaginary axis to the negative side of α and the fixed point becomes stable. Thus it can be seen that for the same value of F, depending on the value of delay, the fixed point can be stable or unstable.

$$\frac{d\alpha}{d\tau}_{\lambda = i\gamma} = \frac{-(K_4)\gamma sin(\gamma\tau)(-K_2 + K_4\tau cos(\gamma\tau)) - K_4\gamma cos(\gamma\tau)(2\gamma - K_4\tau sin(\gamma\tau))}{(-K_2 + K_4\tau cos(\gamma\tau))^2 + (2\gamma - K_4\tau sin(\gamma\tau))^2} \tag{15}$$

3. Simulation and results

Figure 1a shows the plot of τ(n)'s from Eq. (12) plotted against F/I_{th} for the parameter values $I_0 = 1.5$ and $\varepsilon = 0.025$, where I_0 is defined as I_b/I_{th}. Solid curves represent the critical delays with $d\alpha/d\tau$ positive and the dashed curves represent the critical delays with $d\alpha/d\tau$ negative. Substituting Eq. (14) in Eq. (15) we find that $d\alpha/d\tau$ is positive for τ_1 and negative for τ_2 for all values of n. τ_1 and τ_2 for the same value of n join to form closed curves ($\tau_1\tau_2$(n)). Four such closed curves for n equal 1 to 4 are shown in Figure 1a. They exist only for a range of F; outside this range stability does not depend on τ. Moreover, immediately outside this range, α is negative, indicating the fixed point is stable. Figure 1b shows the scan of (F/I_{th}, τ) parameter space, by simulating the laser dynamics with feedback at each point. The shaded area represents points where the solution P(t) converged to a fixed point and the unshaded region represent the points where P(t) is oscillatory. Substituting $\tau = 0$ in the characteristic equation and solving, we find that α is negative at $\tau = 0$ below the curve τ_1 (n = 1). Therefore, the fixed point is stable at $\tau = 0$. Thus the first stability region is the area enclosed between the curves $\tau = 0$ and τ_1 (n = 1). In Figure 1b, this is the shaded region below the first unshaded patch. From τ_1 (n = 1), stability regions are formed between a lower dashed curve and an upper solid curve. Inside the region enclosed by $\tau_1\tau_2$ (n), the fixed point is always unstable because α calculated at the fixed point is always greater than zero, as indicated by the solid lower curves and dashed upper curves. However, at both ends of these curves, where there are no overlaps, stability regions are formed between τ_2(n) and τ_1(n + 1). These are the protruding shaded regions on both sides in Figure 1b. Successive curves overlap to greater extent in the middle and the stability regions are pushed towards both sides, reducing their area. In the simulations it is assumed that the feedback is applied after the laser has stabilized to its steady state. What happens when the feedback is applied before stabilization is discussed in section 3.3. Figure 2 depicts the Hopf bifurcations at the critical delay values. At $F/I_{th} = 0.45$, the first instance of losing stability occurs at the critical value of delay $\tau_c = 0.33$ ns; this point is marked P1 in Figure 1a. Figure 2a shows P(t) at 0.2 ns where $\tau < \tau_c$. When feedback is applied P(t) suddenly stabilizes to the new fixed point with highly damped oscillations. At $\tau = \tau_c$ a periodic solution appears as shown in Figure 2b. When $\tau > \tau_c$, undamped growing oscillations are obtained

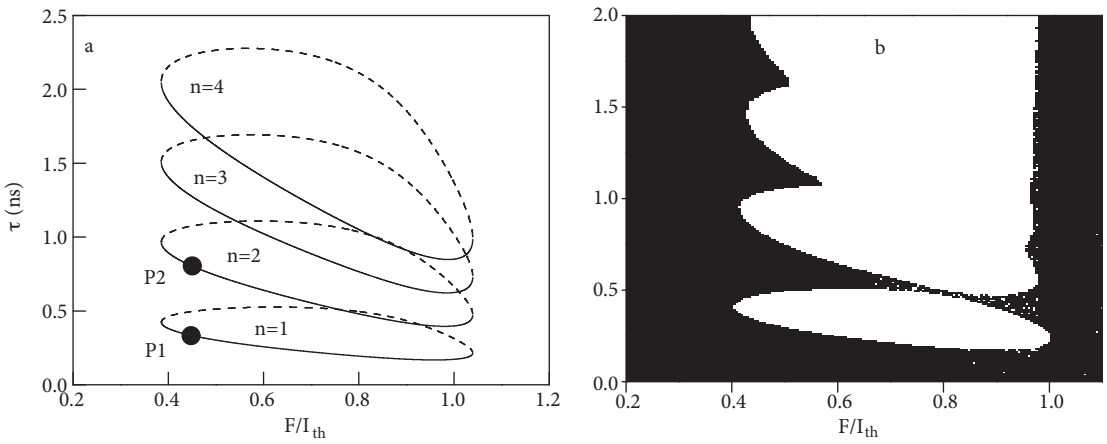

Figure 1. (a) Curves representing Eq. (14) for the parameter values $I_0 = 1.5$ and $\varepsilon = 0.025$ and for n from 1 to 4. Solid curves represent τ_1(n) and dashed curves represent τ_2(n). τ_1 and τ_2 for the same value of n are joined to form closed curves. $d\alpha/d\tau_n$ is positive for τ_1 and negative for τ_2. (b) Stability regions obtained by simulating the dynamical Eqs. (1) and (2). Shaded regions show the points at which the laser goes to a steady state when feedback is applied and the unshaded regions show the points at which the laser goes to an oscillatory state.

(Figure 2c). Figures 2d–2f depict the same scenario across the second instance (marked P2 in Figure 1a) of losing stability at $\tau_c = 0.8$ ns. This numerically verifies the Hopf bifurcation phenomena occurring along the critical delay curves with $\mathrm{d}\alpha/\mathrm{d}\tau$ is positive, that is, on $\tau_1\,(\mathrm{n})$.

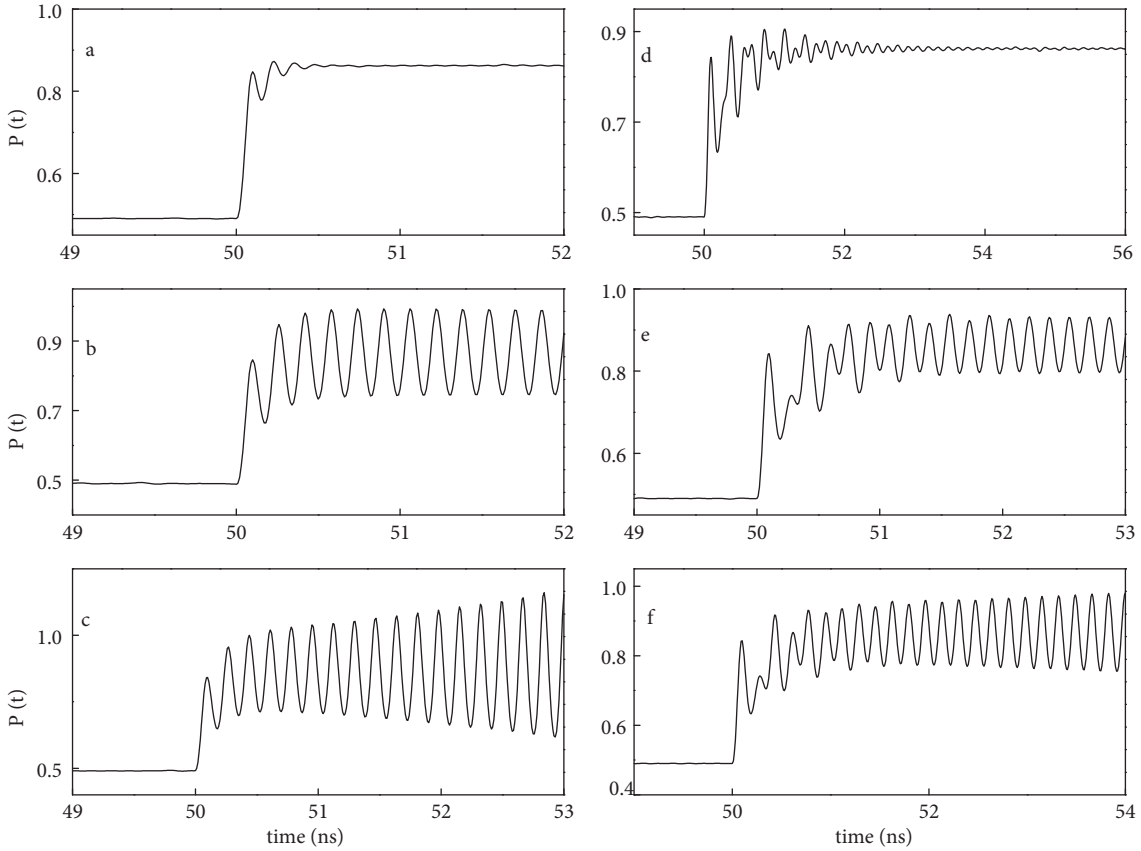

Figure 2. Solution P(t) of the laser dynamical equations when the feedback is applied at t = 50 ns with $\mathrm{F/I}_{th} = 0.45$. (a) Damped oscillatory decay to the fixed point at $\tau = 0.2$ ns. (b) Periodic solution at $\tau = \tau_c = 0.33$ ns. (c) Undamped growing oscillations at $\tau = 0.4$ ns. (d) Damped oscillatory decay to the fixed point at $\tau = 0.75$ ns. (e) Periodic solution at $\tau = \tau_c = 0.8$ ns. (f) Undamped growing oscillations at $\tau = 0.85$ ns. (a),(b), and (c) show Hopf bifurcation happening at $\tau_c = 0.33$ ns and (d),(e), and (f) show the same for $\tau_c = 0.8$ ns.

3.1. Effect of nonlinear gain reduction factor

We show that changes in ε can drastically change the critical delay curves. In Figure 3 delay curves for increasing values of ε are plotted. For small values of ε stability regions are formed only on the lower side of $\mathrm{F/I}_{th}$ except for the first stability region that lies between $\tau = 0$ and $\tau_1\,(\mathrm{n} = 1)$. This result is shown in Figure 3a for the value 0.01 of ε. Here all τ_1's where $\mathrm{d}\alpha/\mathrm{d}\tau_n$ is positive (solid curves) converge closer to the $\tau = 0$ axis for higher values of $\mathrm{F/I}_{th}$ and at least one eigen value has a positive real part above $\tau_1\,(\mathrm{n} = 1)$, on the right end. The span of the curves decreases as ε is increased to 0.02 in Figure 3b, which indicates that delay has a role in determining stability only for shorter ranges of $\mathrm{F/I}_{th}$. With further increase in ε, the curves with $\mathrm{d}\alpha/\mathrm{d}\tau_n$ positive and negative for the same n join at the right end to form closed structures ($\tau_1\tau_2\,(\mathrm{n})$) and stability regions are formed at both ends. At the same time, the extent of overlap between these closed

curves decreases. In Figure 3c, $\tau_1\tau_2(1)$ and $\tau_1\tau_2$ (2) completely move apart from overlap for $\varepsilon = 0.03$ and the stability region becomes continuous between them. More curves move apart as ε is increased and they change to elliptical as shown in Figure 3d. Around $\varepsilon = 0.035$ the curves completely disappear, making the stability of the fixed point independent of τ.

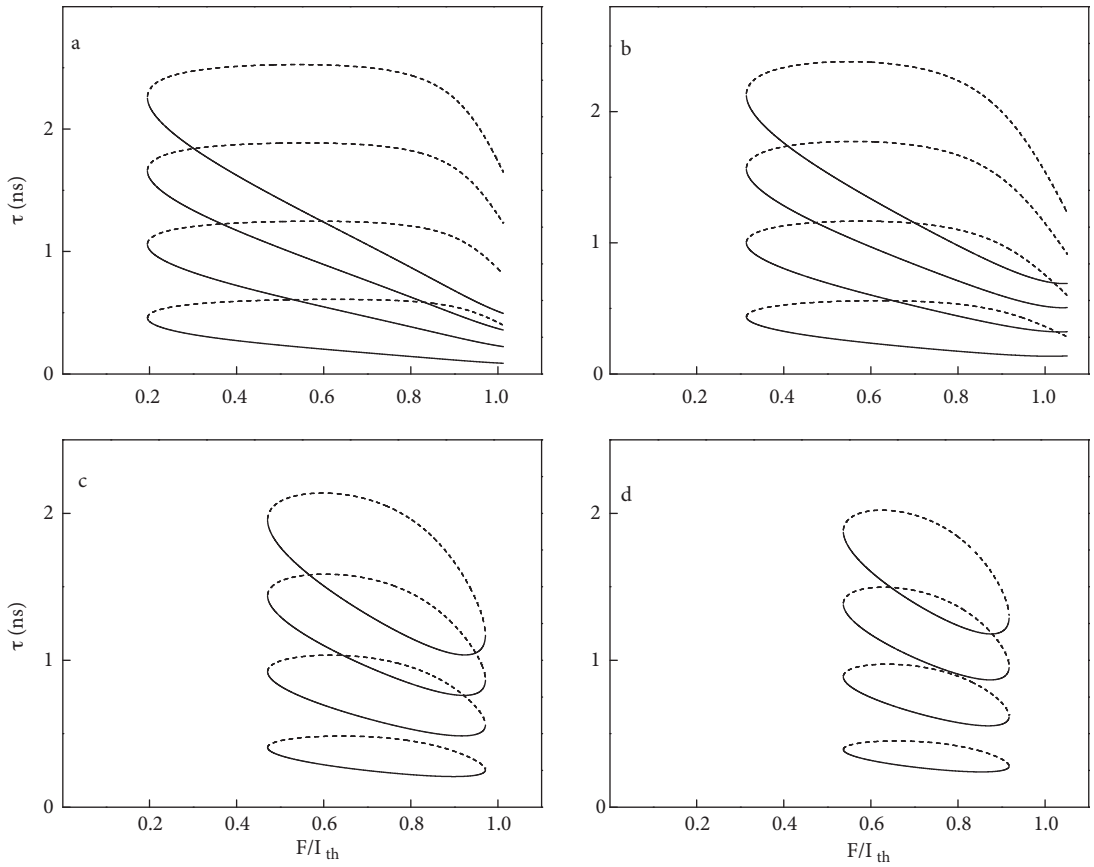

Figure 3. Critical delay curves for 4 different values of ε. (a) $\varepsilon = 0.01$, (b) $\varepsilon = 0.02$, (c) $\varepsilon = 0.03$, (d) $\varepsilon = 0.031$.

3.2. Effect of bias current

Figures 4a–4c show critical delay curves at $\varepsilon = 0.025$ for I_0 equal to 1.4, 1.7, and 1.9, respectively. Increase in I_0 has similar effects as increase in ε. Dependence of stability on delay converges to shorter ranges of F for higher I_0's. The closed curve structures ($\tau_1\tau_2$(n)) change to oval and the extent of overlap between the them decreases. Around I_0 equal to 1.9 four curves move apart and form continuous stability regions between them. As a result of flattening of the curves, for higher I_0 successive Hopf bifurcations come closer in delay. The curves completely disappear before I_0 is increased up to 2.

3.3. Effect of initial condition

Numerical simulations in the previous sections had the assumption that the laser has settled to the steady state before feedback is applied. Thus for the delay differential equations representing the delay feedback dynamics the initial condition is a constant function, namely the steady state solution without feedback. However, situations can arise where this is not the case. Feedback can be present from $t = \tau$, where τ is the delay in feedback. Here,

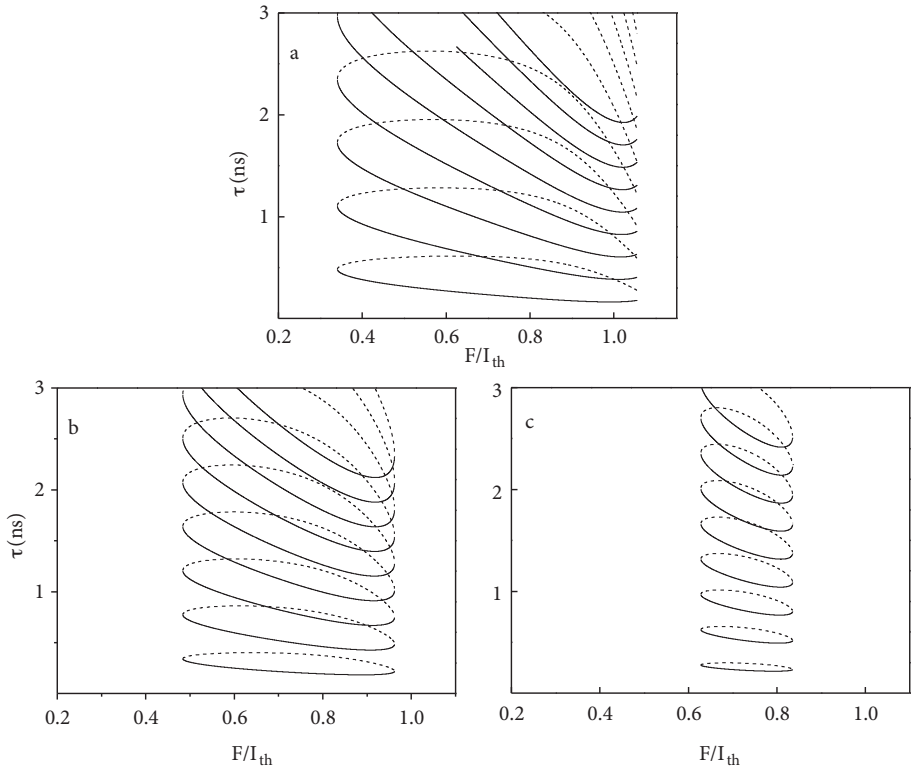

Figure 4. Critical delay curves for 3 different values of I_0. (a) $I_0 = 1.4$, (b) $I_0 = 1.7$, (c) $I_0 = 1.9$.

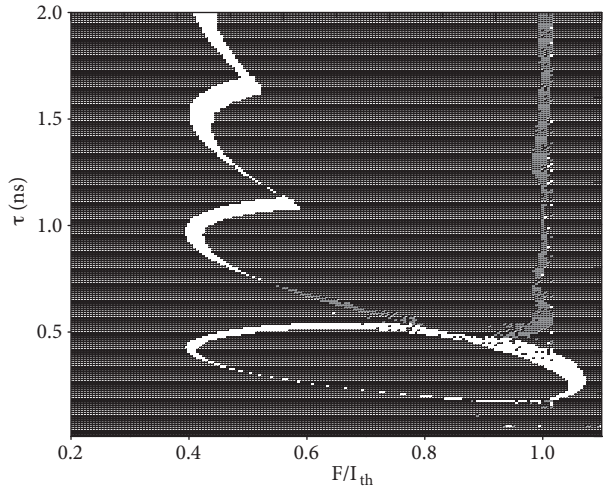

Figure 5. Differences in final states when feedback is applied after the SL is stabilized to the fixed point and before stabilization for the parameter values $I_0 = 1.5$, $\varepsilon = 0.025$. In the completely shaded region the SL goes to the same final state in both cases. In the completely unshaded area, SL goes to a fixed point when feedback is started after the laser is stabilized to the fixed point and to an oscillatory solution when the feedback is started at time $t = \tau$ (delay). In the half-shaded regions the dynamics are switched. The SL goes to an oscillatory state in the first situation and to a fixed point in the second.

if τ is shorter than the time taken by SL to stabilize to the fixed point after relaxation oscillations, the initial function is not a constant. In this scheme the parameter space is divided based on 3 types of behavior: regions where the attractor remained the same as with the previous case, regions where the attractor changed from fixed point to a limit cycle, and regions where the attractor changed from a limit cycle to a fixed point. Figure 5 characterizes the (F/I_{th} ,τ) parameter space for these 3 types of behavior. One such instance for parameter values F/I_{th} = 0.52, I_0 = 1.5, and τ = 1.1 ns is given in Figure 6. In Figure 6a, when the feedback is applied at t = 50 ns, SL is already operating at the steady state, and P(t) settles to the new fixed point after damped oscillations. Figure 6b shows the case when feedback is present from 1.1 ns, which is equal to the delay. In this case P(t) is undamped and slowly growing. Such points are represented by the unshaded regions in Figure 5. If P(t) is oscillatory when the initial feedback function is constant, one would expect the same for a case when the initial feedback function itself is oscillatory, but we get the unexpected result as shown in Figures 6c and 6d. Here the final state is the fixed point when feedback is applied at t = τ (0.53 ns), but the final state is oscillatory when feedback is applied after the stabilization of the SL to the fixed point. The half-shaded regions in Figure 5 represent this behavior.

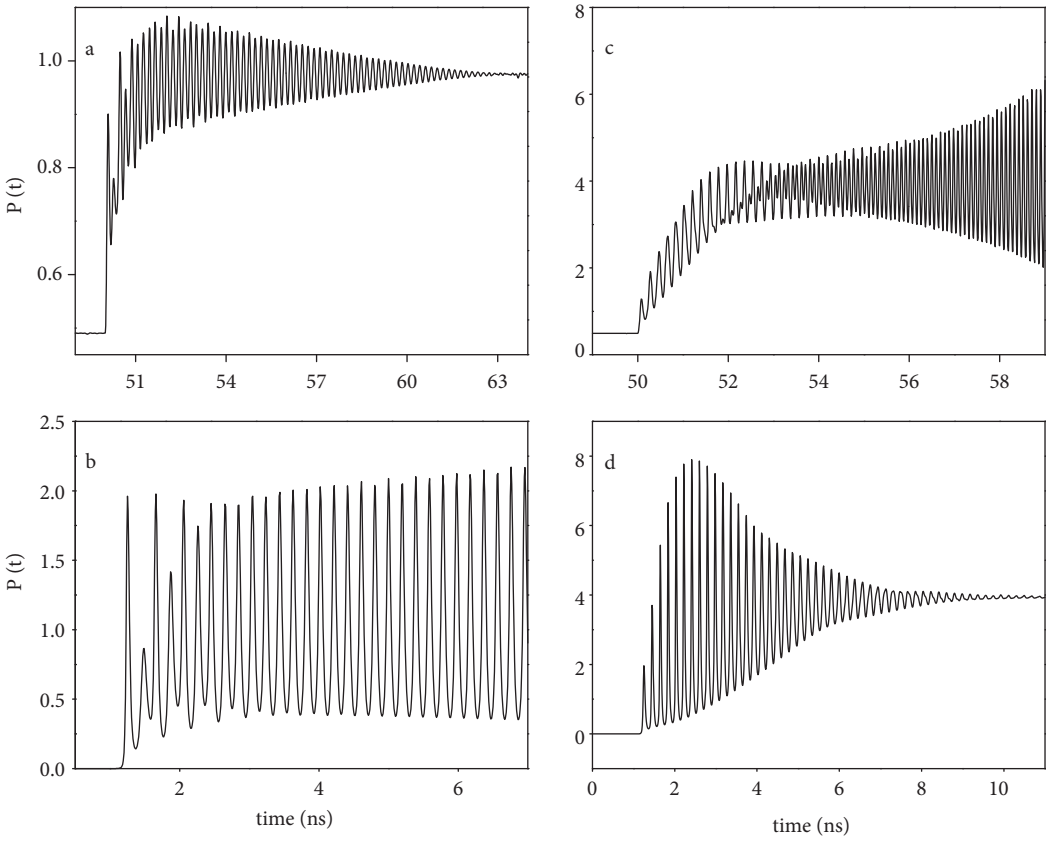

Figure 6. Solution P(t) of the rate equations for 2 different initial conditions for the parameter values F/I_{th} = 0.52, I_0 = 1.5, and τ = 1.1 ns. (a) Feedback is applied at 50 ns when the laser is already operating at its steady state. Dynamics converge to the new fixed point after damped oscillations. (b) Feedback mechanism is present from a time t = τ after the beginning of the operation. Here the solution goes to oscillatory state. (c) and (d) show the final states switched for F/I_{th} = 0.99 and τ = 0.53 ns.

4. Conclusions

We have done the linear stability analysis of the nonlinear delay differential equations arising in a SL with optoelectronic delay feedback. Critical stability curves and Hopf bifurcation points obtained from the analysis are verified by simulating the delay dynamics of the SL. Here simulations are done such that delay feedback is switched on only after the SL has stabilized to the fixed point. Deviations from the predicted behavior, when the feedback is present from the beginning, are discussed. Effects of nonlinear gain reduction factor and bias current are deduced from the analysis and are numerically verified. Increase in both of these parameters reduces the range of feedback strength where the stability depends on delay. Beyond a critical value, stability of the steady state solution becomes independent of delay.

Acknowledgments

Authors Varghese Bejoy and Vadakkedath Madhom Nandakumaran thank the Board of Research in Nuclear Sciences (BRNS), India, for its financial support. The authors thank Manu P John for discussions and suggestions.

References

[1] Soriano, M. C.; Garcia-Ojalvo, J.; Mirasso, C. R.; Fischer, I. *Rev. Mod. Phys.* **2013**, *85*, 421–470.

[2] Weiss, C. O.; Vilaseca, R. *Dynamics of Lasers*, Wiley-VCH: Weinheim, Germany, 1991.

[3] Krauskopf, B. In *AIP conference proceedings: Nonlinear Dynamics: Concepts, Mathematics, Physics, and Applications International Spring School*, Texel, the Netherlands, 16–19 April 2000.

[4] Jiang, G.; Zhang, J.; Huang, Y. *Turk. J. Phys.* **2013**, *37*, 296–303.

[5] Deng, T.; Xia, G.; Wu, Z.; Lin, X.; Wu, J. *Opt. Express* **2011**, *19*, 8762–8773.

[6] Fujino, H.; Ohtsubo, J. *Opt. Rev.* **2001**, *8*, 351–357.

[7] Sacher, J.; Baums, D.; Pankin, P.; Elsasser, W.; Gobel, E. O. *Phys. Rev. A* **1992**, *45*, 1983–1905.

[8] Rajesh, S.; Nandakumaran, V. M. *Physica D* **2006**, *213*, 113–120.

[9] Ludge, K.; Schuster, H. G. *Nonlinear Laser Dynamics: From Quantum Dots to Cryptography, Reviews of Nonlinear Dynamics and Complexity*, Wiley-VCH: Weinheim, Germany, 2011.

[10] Erneux, T.; Glorieux P. *Laser Dynamics*, Cambridge University Press: Cambridge, UK, 2010.

[11] Lakshmanan, M.; Senthilkumar, D. V. *Dynamics of Nonlinear Time-Delay Systems*, Springer-Verlag: Berlin, Heidelberg, Germany, 2010.

[12] Kouomou Y. C. PhD, Department of Physics, University of the Balearic Islands, Palma de Mallorca, 2006.

[13] Lin, F.; Liu, J. *IEEE J. Select. Topics Quantum Electron.* **2004**, *5*, 991–997.

[14] Masoller C.; Cabeza C.; Schifino, A. S. *IEEE J. Quantum Electron.* **1995**, *31*, 1022–1028.

[15] Krauskopf, B.; Gray, G. R.; Lenstra, D. *Phys. Rev. E* **1998**, *58*, 7190–7197.

[16] Sacher, J.; Baums, D.; Pankin, P.; Elsasser, W.; Gobel, E. O. *Phys. Rev. A* **1992**, *45*, 1983–1905.

[17] Vicente, R.; Tang, S.; Mulet, J.; Mirasso, C. R.; Liu, J. *Phys. Rev. E.* **2004**, *70*, 046216.

[18] Agrawal G. P. *Appl. Phys. Lett.* **1986**, *49*, 1013–1015.

[19] Rajesh, S.; Nandakumaran, V. M. *Phys. Lett. A* **2003**, *319*, 340–347.

[20] Lee, T. P.; Burrus, C. A.; Copeland, J. A.; Dental, A. G.; Marcuse, D. *IEEE J. Quantum Electron.* **1982**, *QE-18*, 1101–1113.